Applied Physics A (2026) 132:377
https://doi.org/10.1007/s00339-026-09555-6

Applied Physics A
Materials Science & Processing

Temperature controlled phase transition and characterization of Cu_2O and CuO thin films grown at different growth temperatures via mist CVD

Polat Narin[1] · Ece Kutlu-Narin[2] · Sukru Ardali[3] · Beyza Sarikavak-Lisesivdin[4] · Engin Tiras[5] · Sefer Bora Lisesivdin[4]

Received: 20 December 2025 / Accepted: 24 March 2026
© The Author(s) 2026

Abstract

This study investigates the phase-controlled copper oxide thin films by growth temperature using the mist-CVD methods. The main aim of the study is to determine the phase transition between Cu_2O and CuO crystals in the range of 300 °C and 450 °C. It is found that 300 and 350 °C of growth temperatures showed only Cu_2O cubic crystal phase, 400 and 450 °C of growth temperatures observed only CuO monoclinic crystals, confirmed by X-ray diffraction (XRD) and Raman spectroscopy measurements. A unique boundary in the crystal phase transition between Cu_2O and CuO was shown. It was found to be an important parameter of the growth temperature to adjust the phase transition between CuO and Cu_2O. The morphological examinations revealed by atomic force microscopy (AFM) and scanning electron microscopy (SEM), show that the surface roughness and grain shape are utilized to determine the phase transition. The optical properties from the UV-visible spectrophotometer show that the optical band gaps are reduced from 2.45 eV (Cu_2O) to 1.38 (CuO) because of the phase transition. The low-temperature PL measurement is considered to provide insight into the defect structure and phase transition in Cu_2O and CuO. The obtained results show that the growth temperature is a very effective way to control the phase transition between Cu_2O and CuO crystals.

Keywords Cu_2O · CuO · mist CVD · optical properties

1 Introduction

Nowadays, metal oxides have been considered a significant group of functional materials owing mainly to their tunable electronic properties, cost-effective preparation methods, thermodynamic stability, and stoichiometric diversity [1, 2]. Their semiconductor behavior is more essential for stability than their metallic counterparts. Metal oxide materials, when well prepared, such as having a high crystalline quality, high optical transparency, and high electron/hole mobility, have become a good candidate for optoelectronic, sensing, and photocatalytic applications [3–5]. Copper oxide is distinct from other metal oxides because it has two main stable phases, which are related to the oxidation state of the copper atom. One of these is copper (I) oxide (Cu_2O), named as cuprous oxide and the other is copper (II) oxide, CuO, named as cupric oxide. Both crystals show p-type semiconductor behavior, having a range of 1.2 eV-2.1 eV of

✉ Polat Narin
polatnarin@aybu.edu.tr

1 AYBU Central Research Laboratory, Ankara Yildirim Beyazit University, Ankara 06010, Türkiye

2 Graduate School of Natural and Applied Sciences, Ankara University, Ankara 06100, Türkiye

3 Department of Electricity and Energy, Porsuk Vocational School, Eskişehir Technical University, Odunpazarı, Eskişehir 26140, Türkiye

4 Faculty of Science, Department of Physics, Gazi University, Teknikokullar, Ankara 06500, Türkiye

5 Department of Physics, Faculty of Science, Eskişehir Technical University, Yunus Emre Campus, Eskisehir 26470, Türkiye

Published online: 07 April 2026

energy band gap in CuO and a range of 2.1–2.6 eV of the energy band gap in Cu_2O [6, 7].

The phase transition between Cu_2O and CuO strongly relied on growth methods and growth parameters such as pressure, annealing post-process, growth temperature, laser heating, etc [8–11]. The oxygen ratio in the atmosphere is responsible for the phase transition from Cu_2O to CuO, apart from growth temperature. Although the formation of CuO crystals instead of Cu_2O is increasing with increment in growth temperature [12], Cu_2O crystals can still be grown at 700 K (~426 °C) under vacuum [13]. Therefore, in order to determine the transition temperature is very difficult because each growth method has its own unique characteristics, such as the use of vacuum, solution, or gas phase precursors. Moreover, as mentioned above, the annealing process in the Cu_2O/CuO system is one of the most effective phase transition control mechanisms [14]. The oxidation state of the Cu atom is strongly dependent on ambient temperature, and the Cu^{2+}, which exhibits thermodynamically favorable properties, is responsible for the formation of CuO crystals. To form Cu_2O, the reduction oxidation state from Cu^{2+} to Cu^{+} and additional energy are required.

Metal oxide materials are grown by different growth methods such as chemical vapor deposition (CVD), RF-DC magnetron sputtering, spray pyrolysis, sol-gel process, mist-CVD, etc [15–22]. Among these growth methods, solution-based methods are very useful, having cost-effective, easy-to-grow thin films, and non-required vacuum equipment. The mist-CVD method is also a CVD method that uses a solution precursor instead of a gas phase. Control parameters such as gas flow rate, growth temperature, and precursor molarity are equipped in the mist-CVD system. For instance, Ikenoue et al. have successfully grown Cu_2O thin films that exhibited a high hole mobility [23]. The high hole mobility in Cu_2O makes it a promise for transparent power electronic applications. Moreover, the mist-CVD method is a strong candidate for epitaxial film growth particularly oxide thin films.

This study investigates phase control in the Cu_2O and CuO thin films grown by the mist-CVD method. In the thermodynamic phase transition between Cu_2O and CuO, the effect of growth temperature on physical properties and growth behavior of Cu_2O and CuO thin films is systematically studied. Before the growth of the films, the used chemical copper (II) acetylacetonate ($Cu(acac)_2$) is decomposed by thermogravimetric analysis (TGA) to determine the start point of growth temperature. The phase transition between the grown films is uniquely determined by the change in the structural, morphological, and optical properties of Cu_2O and CuO thin films. The crystal phases and morphological properties of Cu_2O and CuO thin films are evaluated by XRD, AFM, and SEM measurements. The defect structure, optical and vibrational properties of these films are investigated using Raman, UV-visible optical spectrophotometer, and low-temperature PL measurements.

2 Experimental methods

Cu_2O and CuO thin films were grown on glass substrates using the mist-CVD method. The $Cu(acac)_2$ powder was dissolved in deionized water (DIW) to prepare a 0.05 M precursor solution and to increase the homogeneity of the prepared precursor solution, the same ratio of Ethylenediaminetetraacetic acid (EDTA) like $Cu(acac)_2$ was added to the prepared precursor solution. The pH value of the precursor solution was kept at 10 from our previous study [22]. Before growth, the reactor was kept under N_2 atmosphere, and during growth, N_2 with 1000 ml/minutes as a carrier gas and O_2 with 100 ml/minutes as an oxidation gas were conveyed to the reactor for 90 min, which is the growth time. Mist vapors, including copper ions, were formed by a 1.7 MHz ultrasonic transducer. To ensure a hidrophilic surface of the glass, a mixture of sulphuric acid (3:1) and hydrogen peroxide was applied to substrates for 30 min. The determination of the growth temperature was obtained using TGA of $Cu(acac)_2$ powder as given in Fig. 1. The decomposition process of $Cu(acac)_2$ starts near 225 °C, which is the onset temperature of $Cu(acac)_2$ and it ends completely near 260 °C. It was seen that a single step decomposition of $Cu(acac)_2$ existed, and there was no other intermediate step during the decomposition process. This result is also confirmed by the literature and the results reveal that the sublimation TEMPERATURE IS FOUND TO BE 266 ºC [24]. Because $Cu(acac)_2$ powder still exists before 260 °C, the growth temperature of Cu_2O and CuO thin films for the lowest limit in the mist-CVD method is chosen as 300 °C. Growth temperatures of Cu_2O and CuO thin films were determined to be 300 °C, 350 °C, 400 °C, and 450 °C.

Structural characterization of grown Cu_2O and CuO was examined by thin film XRD measurement with Rigaku Miniflex 600. In XRD measurements, the Bragg-Brentano geometry was used. Surface properties of thin films were investigated using AFM (TT-2 AFM workshop) and field emission SEM (Hitachi SU5000) equipped with an energy dispersive X-ray spectrum (EDS) detector (Oxford X-max 80). The optical properties of thin films were studied using a UV-visible spectrophotometer (Shimadzu 1700). The vibrational properties were also examined by the confocal Raman system (Jasco NRS-4500).

PL measurements were performed as a function of temperature ranging from 3 to 300 K. The samples were placed in a closed-cycle helium-cooled cryostat (Oxford Optistat Dry) under vacuum, and the optical excitation source was a

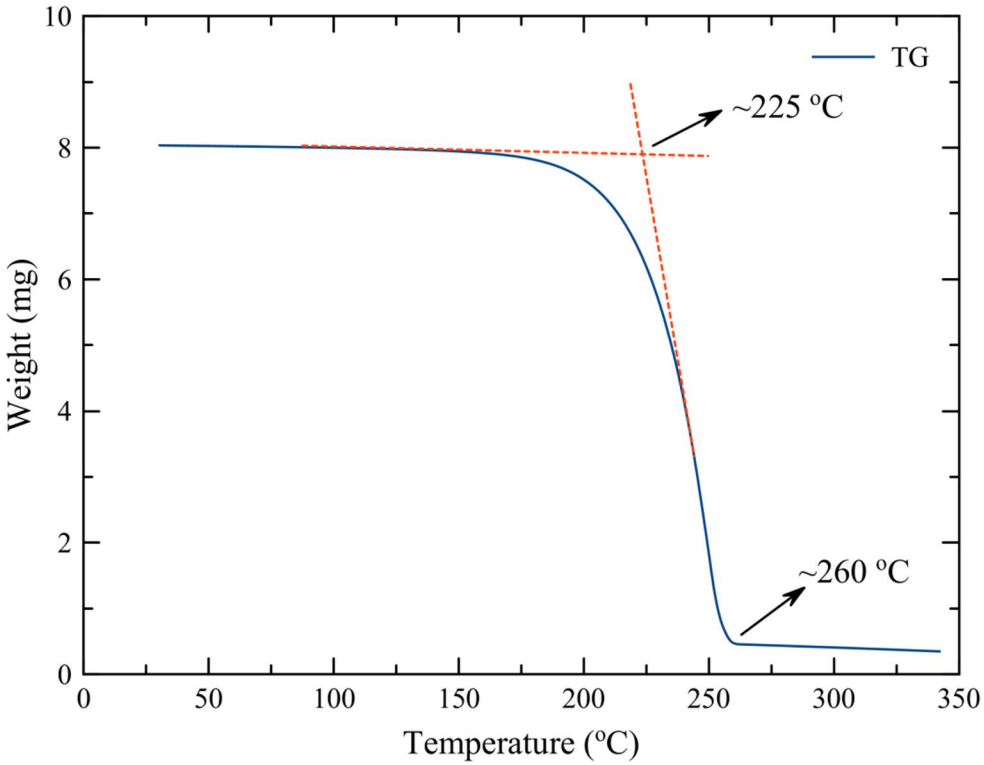


Fig. 1 TGA curve of copper (II) acetylacetonate as the starting material

325 nm helium–cadmium laser (Kimmon IK3102R-G, 100 mW power output). The PL signals from the samples were detected using a thermoelectrically cooled Newton 970 electron-multiplying charge-coupled device (EMCCD) detector in combination with an Andor SR500i spectrograph.

3 Results and discussion

Figure 2 shows the XRD pattern of the grown thin films. It is clearly seen that 300 and 350 °C of growth temperature only formed Cu_2O crystals. The Cu_2O crystals grown at these temperatures exhibit a cubic polycrystalline structure but have a highly dominant (111) diffraction at 36.46°. Also, they observe low intensity with (200) and (110) diffractions at 29.66° and 42.26°, respectively. In the case of 400 and 450 °C of growth temperature, only CuO crystals with monoclinic polycrystalline behaviour are formed. Any peaks belonging to Cu_2O crystals are encountered. The dominant peaks are determined to be (-111)/(002) and (200)/(111) diffractions at 35.62° and 38.82°, respectively. A mixed phase of Cu_2O and CuO has not been seen in these growth temperatures. There are clear boundaries between Cu_2O and CuO crystal formation for the used temperatures. XRD results indicate that only Cu2O crystals can be grown below 350 °C. This result is very similar to that of Cu_2O thin films grown by the same method [23]. The obtained results from the XRD pattern of Cu_2O and CuO thin films are consistent with results found in literature [25, 26]. The thermodynamic stability and phase transition of the Cu_2O/CuO system are mainly controlled by two parameters, O_2 pressure (P_{O2}) and growth temperature [27]. Particularly, Kaur et al. observe that the increasing P_{O2} leads to a transition to CuO. Similarly, we have obtained the effect of the increasing growth temperature on the transition to CuO from Cu_2O in our study. While Kaur et al. have specialized in P_{O2} on the oxidation kinetics in the copper oxide, our study shows a temperature-driven phase transition [8]. Using diffraction peaks in Fig. 2, the lattice parameters of the thin films are estimated and presented in Table 1. The crystallite sizes of Cu_2O and CuO thin films are calculated using the Scherrer equation given by Eq. (1)

$$D = \frac{0.9\lambda}{\beta \cos\theta} \tag{1}$$

where D is crystallite size, λ, β, and θ are 1.54 Å, which is the x-ray wavelength of $Cu\text{-}K_\alpha$, full width at half maxima (FWHM), and peak position of the related peak in XRD pattern. The crystallite sizes of grown thin films are changed between 20 nm and 27 nm for different growth temperatures.

The surface properties of Cu_2O and CuO are determined using AFM and SEM measurements. From the AFM measurement, it can be seen that a relatively uniform surface morphology is found on the surface. The growth temperature of thin films affects the surface morphology and changes the

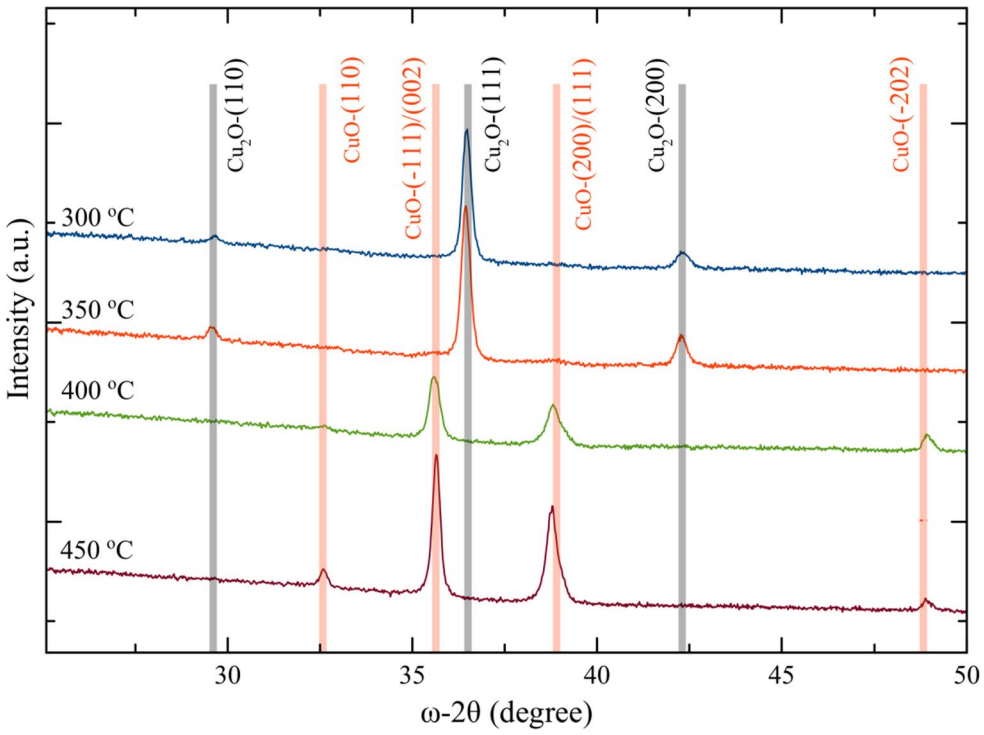


Fig. 2 XRD pattern of Cu_2O and CuO thin films

Table 1 Structural and optical parameters of grown Cu_2O and CuO thin films

Growth Temperature (°C)				
Parameter 300		350	400	450
a (Å)	4.261	4.265	4.701	4.701
b (Å)	4.261	4.265	3.312	3.339
c (Å)	4.261	4.265	5.109	5.102
d_{111} (Å)	2.460	2.462	2.318	2.319
D (nm)	25	27	20	25
Film thickness (nm)	~380	~520	~420	~480
RMS (nm)	41.5	25.3	43.8	41.1
Band gap (eV) Direct transition	2.44±0.01	2.41±0.01	1.35±0.03	1.39±0.04
Band gap (eV) Indirect transition	-	-	1.09±0.09	1.15±0.03
Cu/O ratio at atomic percentage	1.97	1.53	0.86	0.93

surface roughness of the films. The root mean square (RMS) values of the thin films are found to be 41.5 nm, 25.3 nm, 43.8 nm, and 41.1 nm for 300 °C, 350 °C, 400 °C, and 450 °C of growth temperature, respectively Fig. 3.

Relatively, the grown thin films have a rough surface but an RMS of less than 50 nm. AFM images also confirm the presence of large grains on the surface, with diameters of approximately 500–700 nm. However, Cu_2O thin film grown at 350 °C is more uniform and has smaller grains compared with the other films and has lower surface roughness. Also, the surface height profiles of the thin films can be seen on the AFM images. To better understand the surface morphology of grown thin films, field emission SEM (FE-SEM) measurements are carried out, and top views of the surfaces are presented in Fig. 4. The Cu_2O and CuO thin films have a relatively uniform surface. The Cu_2O grown at 300 °C possesses a triangular surface with a facet of {111} in the insert figure of 300 °C. This is caused by higher surface energy than facets of {100} or {200} in Cu_2O cubic crystal [28].

Moreover, XRD results are strongly supported by FE-SEM results. With an increase in the growth temperature, the CuO crystal, which is a stable phase, has started to grow. The grain boundaries of CuO thin films are apparent, and individual grains are formed. The crystallite sizes obtained from the XRD pattern are found to be lower than those obtained from the SEM and the AFM surface images. The presence of sub-grains in the grown films is mainly caused by the difference in the crystalline size. It can be said that the grains seen from AFM and SEM are formed by the different crystallites. These findings are also supported by results found in the literature [29].

The thicknesses of thin films are determined via cross-section FE-SEM images. Because the samples were grown on a glass substrate, before the imaging process, approximately 3–5 nm of gold was coated on the cross-sectional area of the thin films. The films are shown to have homogeneous thickness and their thickness are found between

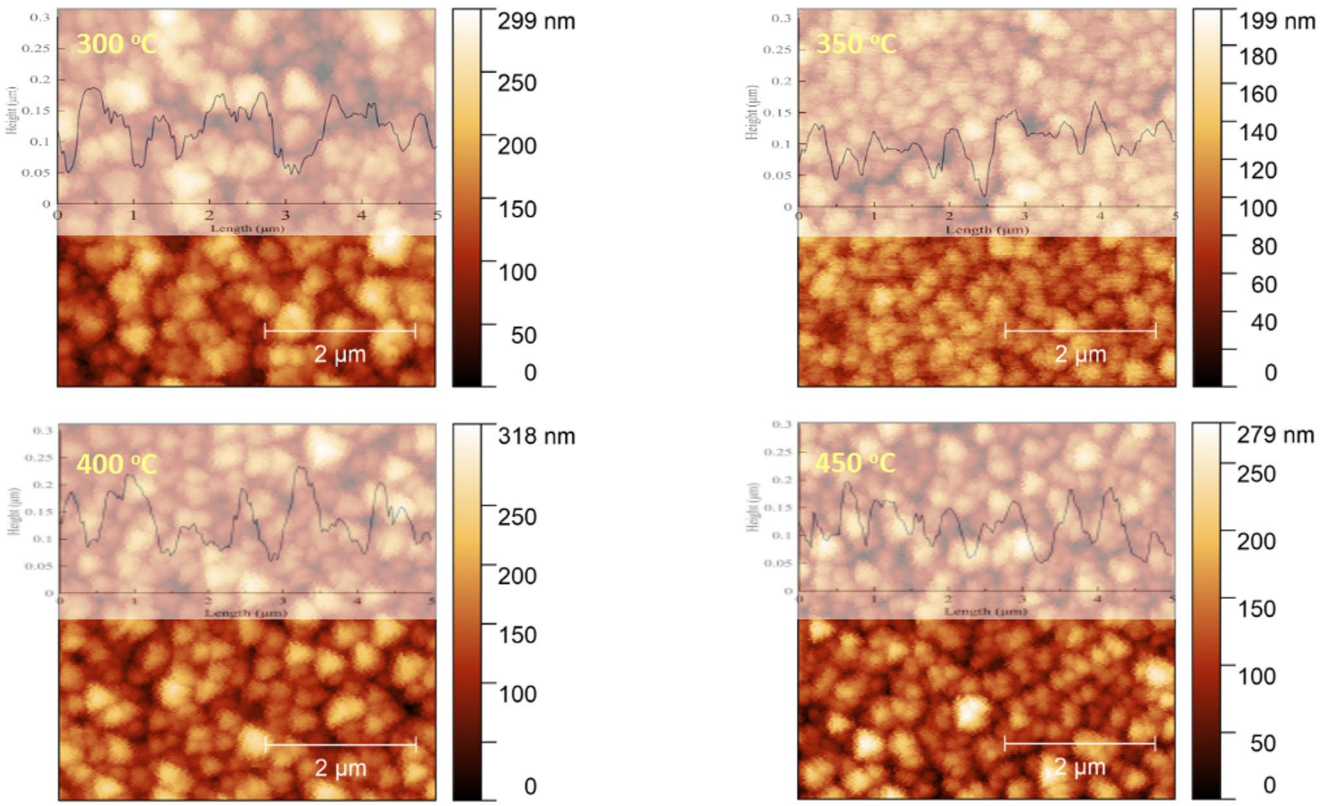


Fig. 3 AFM images of Cu_2O and CuO thin films

350 nm and 550 nm. EDS results show that the atomic ratio of Cu/O at atomic percentage is decreased with increasing growth temperature of the thin films because of the phase transition of the crystals from Cu_2O to CuO. The atomic ratios of Cu/O in the thin films are listed in Table 1.

The vibrational properties of Cu_2O and CuO thin films are investigated in the Raman spectrum given in Fig. 5. The Raman measurement was taken at a range of 100–800 cm^{-1}. The Cu_2O crystal has 18 vibrational modes, but 15 of these are optical modes. The symmetries of the vibrational Raman modes are given by $A_{2u}+E_u+T_{2u}+T_{2g}+3T_{1u}$ [30, 31]. The Cu_2O thin films grown at 300 °C and 350 °C have been shown only Cu_2O phase formation according to the existence of clear peaks located at 145 cm^{-1} and 218 cm^{-1} assigned to Raman active mode $(LO)T_{1u}$ and $2E_u$, respectively, in Cu_2O crystal symmetry. The multi-phonon process appears at 414 cm^{-1} and the four-phonon mode of Cu_2O is located near 620 cm^{-1}. T_{1u} originates from stretching and bending modes of asymmetric Cu-O and O-Cu-O bonds [31]. The CuO crystal has $A_g+2B_g+4A_u+5B_u$ of vibrational symmetry as known in literature [31, 32]. The CuO thin films grown at 400 °C and 450 °C have strong A_g Raman peaks located at 293 cm^{-1}. The CuO thin films also have Raman peaks located at 340 cm^{-1} and 630 cm^{-1} which can be attributed to $B_g^{(1)}$ and $B_g^{(2)}$.

The optical properties of Cu_2O and CuO thin films grown at different temperatures are presented in Fig. 6 as absorbance and transmittance spectra. According to the absorbance spectrum, the absorption edges of thin films shift to longer wavelengths as the growth temperature increases, due to a phase transition from Cu_2O to CuO. From the transmittance spectrum, $Cu_2$2O thin films grown at 300 °C and 350 °C become transparent beyond 500 nm. Maximum transparency is measured as nearly 70% at 750 nm in Cu_2O thin film grown at 300 °C. CuO thin films grown at 400 °C and 450 °C almost exhibit visible-blind optical properties. The maximum transparency for CuO thin films is shown as nearly 70% at 960 nm in the film grown at 450 °C. Using the absorbance spectrum, the optical band gap values of each film are calculated via Tauc's method, given by Eq. (2)

$$(\alpha\, ?\nu\,)^2 = (?\nu\, - E_g) \tag{2}$$

According to Tauc's equation, α and $h\nu$ represent the absorption coefficient and the photon energy, and E_g is the energy band gap. The band gap values of Cu_2O thin films grown at 300 °C and 350 °C are found to be 2.44±0.01 eV and 2.41±0.01 eV using the standard deviation method, respectively. The direct band gap values of CuO thin films grown at 400 °C and 450 °C are calculated as 1.35±0.03 eV and

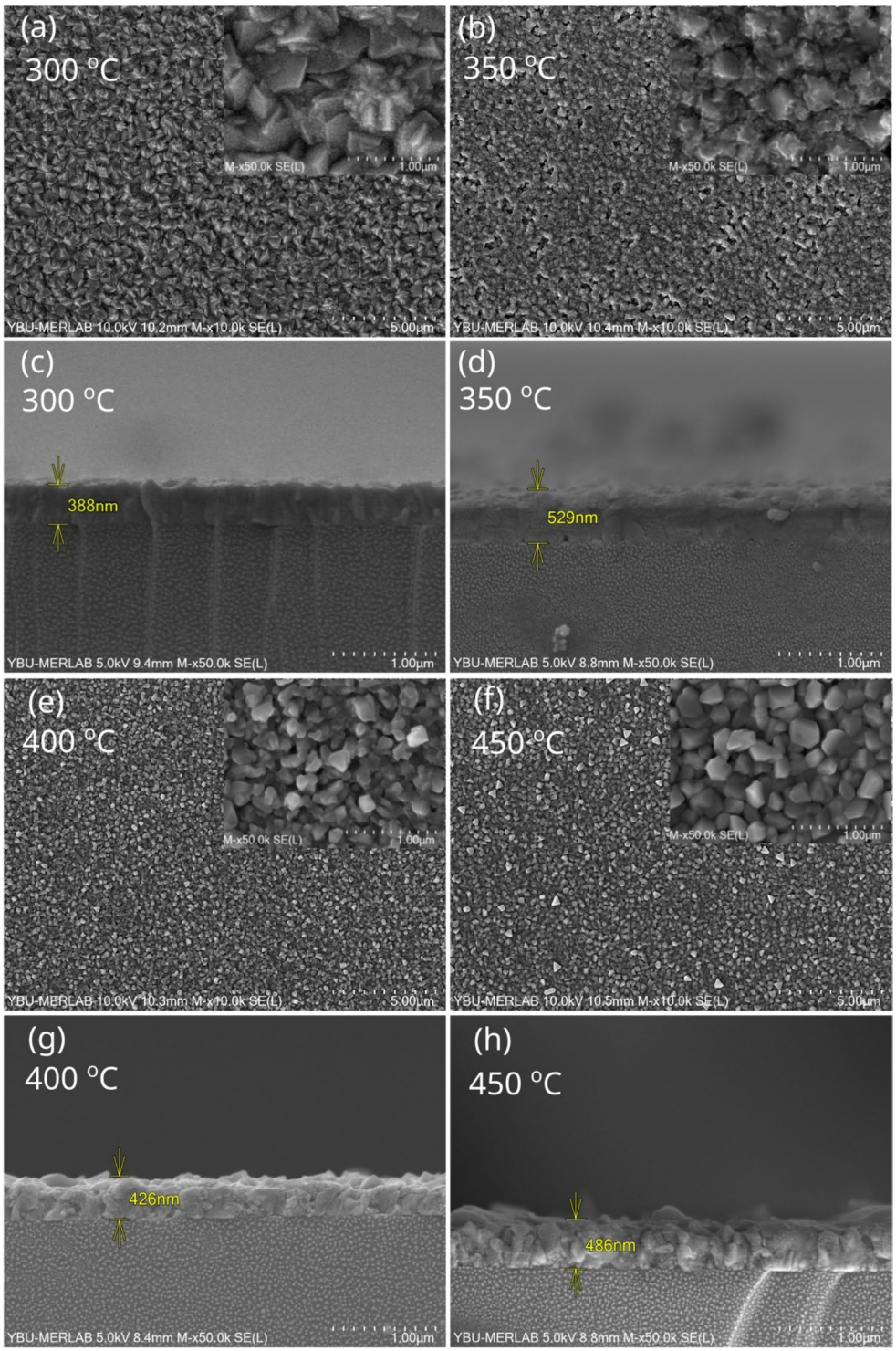


Fig. 4 SEM images of Cu_2O (**a**-**d**) and CuO (**e**-**h**) thin films

1.39±0.04 eV using the standard deviation method, respectively. The CuO shows an indirect band gap, as shown in the literature. The indirect band gaps of CuO thin films grown at 400 °C and 450 °C are found to be 1.09±0.09 eV and 1.15±0.03 ev using the standard deviation method, respectively. for the cuo crystals in the literature, very different optical band gap values are found as 1.21 ev and 1.71 ev, prepared by the rf sputtering method [33, 34]. these contrast results provide information about the growth parameter dependency, even though the same growth method is used to prepare the same crystal. These optical band gaps are consistent with other values found in the literature [35–37] (Fig. 7).

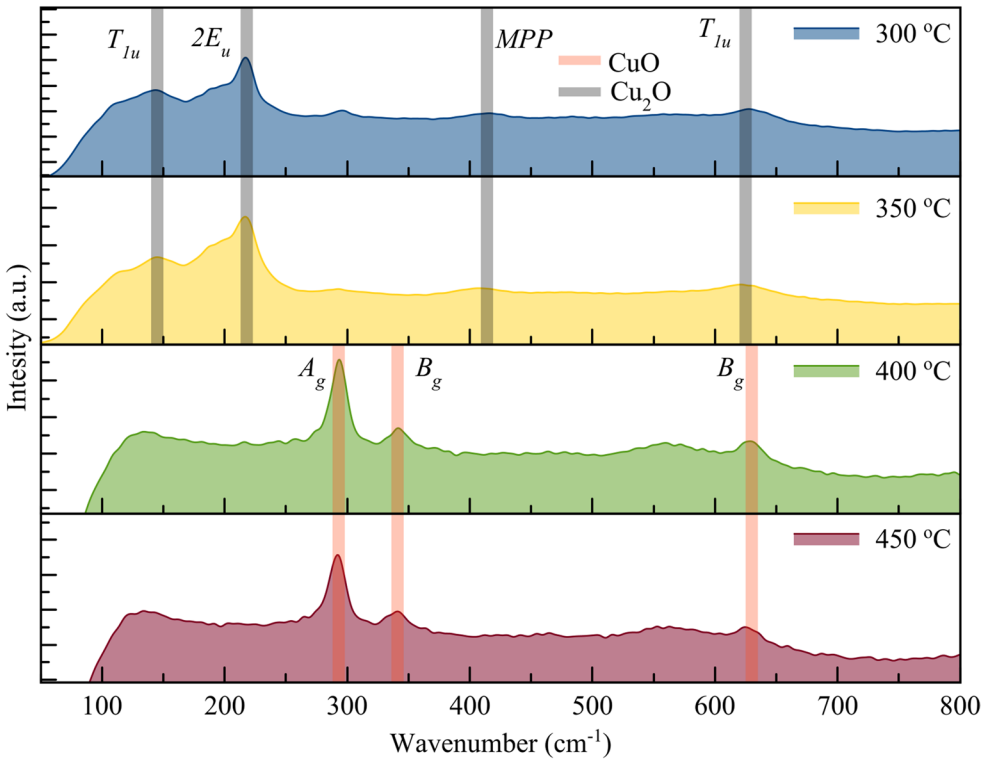


Fig. 5 Raman spectrum of Cu_2O and CuO thin films

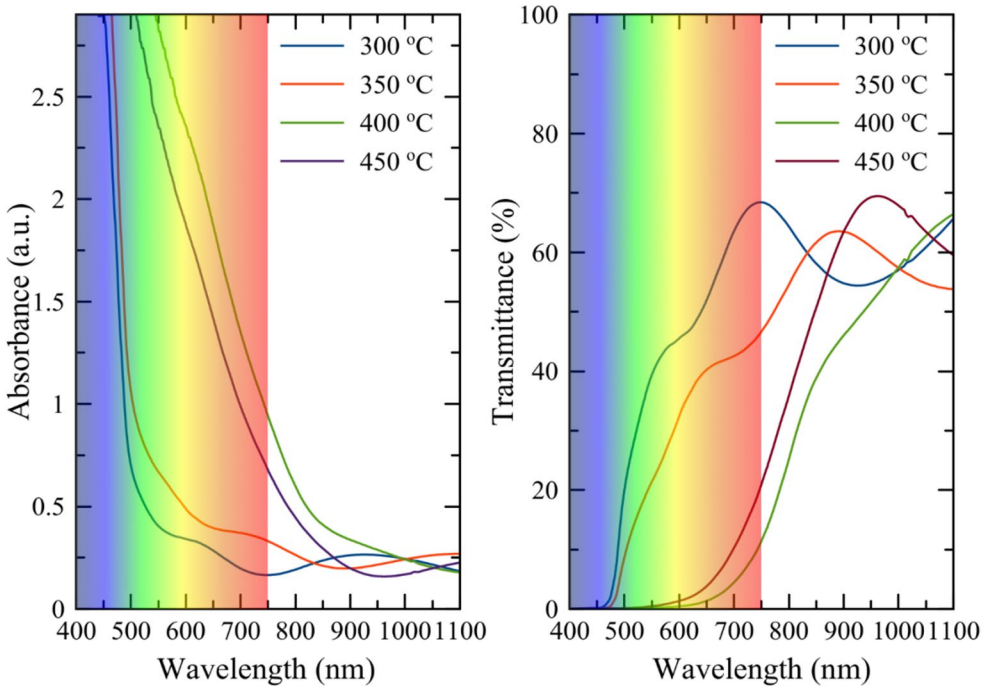


Fig. 6 (**a**) Absorbance and (**b**) Transmittance spectrum of Cu_2O and CuO thin films

Both structural and optical characterizations show that 300 °C and 350 °C of growth temperature are suitable to prepare Cu_2O thin films and 400 °C and 450 °C of growth temperature are also found to obtain only the CuO phase without Cu_2O. To show this phase change between Cu_2O and CuO. Figure 8 is summarized in terms of the lattice parameter and optical band gap of thin films. Depending on the growth temperature, step by 50 °C, while lattice parameters of thin films grown at 300 °C and 350 °C still remain the same, the lattice parameters of other structures are decreased and consistent with the CuO phase. Also, similar behavior is shown in the change of the optical band gap of thin films.

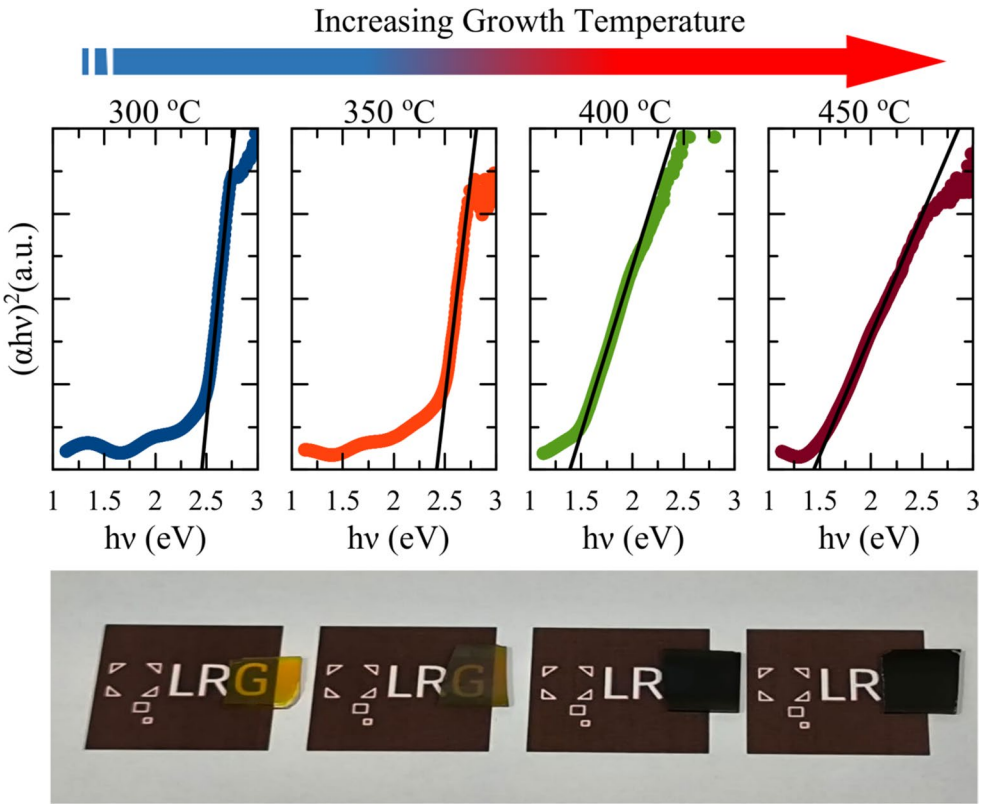


Fig. 7 Tauc's plot of Cu_2O and CuO thin films and pictures of the samples

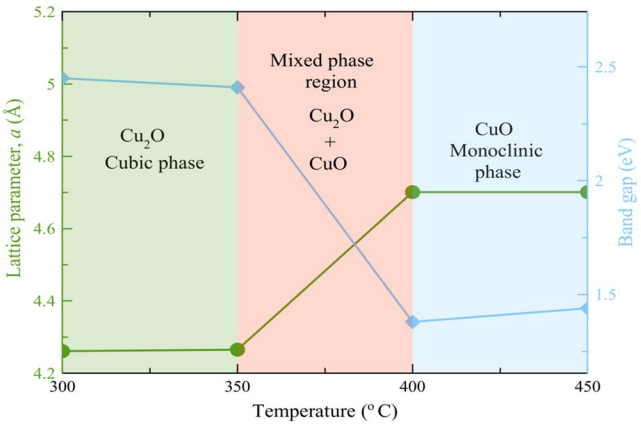


Fig. 8 Change of lattice parameter and optical band gap related to growth temperature

It can be said that the region between 350 °C and 400 °C is where the mixing of Cu_2O and CuO phase transition occurs.

PL measurements taken at 3 K are presented in Fig. 9. Cu_2O thin film grown at 300 °C shows a weak peak located at 563 nm corresponding to near band edge emission (NBE) of Cu_2O. The left shoulder peak of NBE in Cu_2O is located near 532 nm and the peak is attributed to the limit of the green exciton associated with the interband transition $\Gamma_8^+ \rightarrow \Gamma_9^+$ [31]. The highest peak located near 720 nm is attributed to doubly-ionized oxygen vacancies (V_O^{2+}) [38, 39]. It can be said that oxygen-related defects dominate the PL spectrum. Cu_2O thin film grown at 350 °C is shown to have high peak intensity located at 561 nm related to NBE of Cu_2O. The second peak appears at near 720 nm associated with V_O^{2+}. Grown CuO thin films at 400 °C and 450 °C show broad peaks in the PL spectrum. A broad peak centered near 500 nm is shown in CuO thin film grown at 400 °C.

The broad peak with 486 nm and 502 nm can be attributed to blue emission, which results from deep-level transition of interstitial and vacancy cases of oxygen and green emission related to singly ionized oxygen vacancies (V_O^+) [40, 41]. CuO also shows near infrared red (NIR) emission after 700 nm wavelength. A broad emission peak starts from 700 nm to 900 nm and is centered at around 800 nm. The broad emission peak may be assigned a combination of point defects involving copper vacancies, surface-related states, and interstitial defects in the copper oxide rather than a single specific defect type. Furthermore, CuO thin film grown at 450 °C observes similar broad peaks in the PL plot. Determining the NBE of CuO thin films is very difficult due to the presence of deep or shallow levels in the energy band. Moreover, due to p-type semiconductor conductivity defect structure is expected in Cu_2O and CuO thin films, because Cu vacancies in the crystal are responsible for the formation of p-type conductivity [42, 43].

Whereas the oxygen-related defects have a radiative emission at visible and near infrared emission, the Cu vacancies release non-radiative emission and often may not

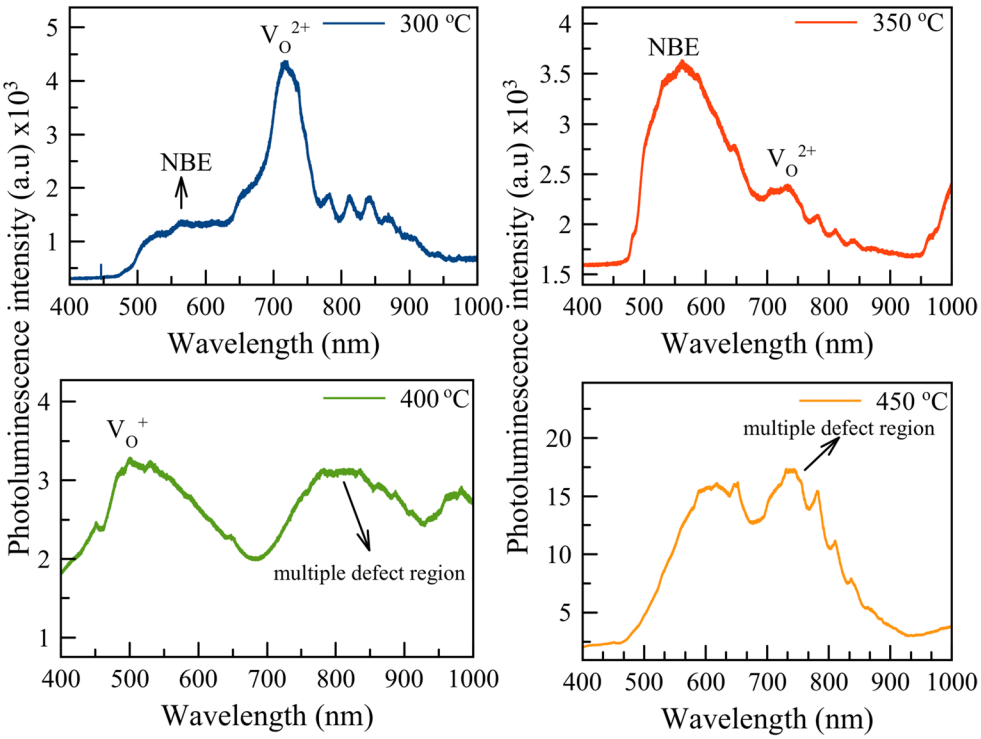


Fig. 9 PL spectrum taken at 3 K of Cu_2O and CuO thin films

be a clear emission peak [44]. The ratio of NBE intensity and defect intensity provide information about crystal quality. The I_{NBE}/I_{defect} ratios for Cu_2O grown at 300 and 350 °C are found to be 0.29 and 1.55, respectively. An increment in the I_{NBE}/I_{defect} is seen in Cu_2O grown at 350 °C better than other Cu_2O crystals in terms of crystal quality. With the increasing growth temperature, the crystal defects, particularly oxygen defects, are filled due to the increasing thermal energy resulting from the growth temperature. Regarding CuO thin films grown at 400 ° C and 450 ° C, it is too hard to determine nbe and defect peak position from pl spectra due to broadened peaks. therefore, we conducted the area integration analysis of defect-related broad peaks between 700 nm and 900 nm in pl spectra. the ratio of these defect areas corresponding to 400 oc and 450 oc is found to be 0.992. it can be said that the growth temperature does not noticeably affect the defect populations in cuo thin films. regarding cuo thin films grown at 400 oc and 450 oc, it is too hard to determine nbe and defect peak position from pl spectra due to broadened peaks. therefore, we conducted the area integration analysis of defect-related broad peaks between 700 nm and 900 nm in pl spectra. the ratio of these defect areas corresponding to 400 oc and 450 oc is found to be 0.992. it can be said that the growth temperature does not significantly affect the defect populations in cuo thin films. the pl spectra are deeply given about the intrinsic electronic structure of the crystals. while cu2o has a fully filled electronic 3d10 configuration, cuo shows an open-shell with a 3d9 configuration in its electronic structure [45]. the differences in the nature of the electronic structure of cu2o and cuo have led to the formation of sub-band gaps in the electronic band structure of cuo [46]. these sub-bandgaps in the energy states may be explained by the broadening defect-related peaks in pl spectra. these energy states can mask the nbe emission compared to the cu2o crystal.

4 Conclusion

In this study, copper oxide thin films are grown at different growth temperatures using the mist-CVD method. Polycrystalline Cu_2O and CuO thin films are grown on glass substrates and the mixed phase of Cu_2O and CuO is not formed at the chosen growth temperature. The surface morphology and thicknesses of thin films are determined by AFM and SEM measurements. The Raman measurement also verified the formation of Cu_2O and CuO crystals. The maximum optical transparencies of Cu_2O and CuO thin films are measured at 70% at 700 nm for Cu_2O grown at 300 °C and 960 nm for CuO grown at 450 °C. While the absorption edge of Cu_2O thin films is in the visible region, that of CuO thin films is shifted to the near infrared region. Using absorbance, the optical energy band gap values are also calculated via Tauc's equation. To investigate the defect structure of thin films, PL measurements are taken at 3 K and the results give good information about defects such as singly or doubly oxygen vacancies or copper vacancies in mist-CVD-grown Cu_2O and CuO thin films. The ability

to uniquely control the phase transition boundary in Cu_2O and CuO crystals as reliable are successfully determined. The controlling phase transition may play a role in power and optoelectronic applications as a p-type material. In the future, the evaluation of the electrical characterizations in pure phases of Cu_2O and CuO and mixed phases of these materials may be better for many application areas. The mist-CVD method will meet a wide range of different types of materials from the perspective of the epitaxial growth.

Acknowledgements This work was supported by Gazi University BAP under project no FGA-2022-7619.

Author contributions Conceptualization: [Polat Narin], [Ece Kutlu Narin]; Methodology: [Polat Narin], [Ece Kutlu Narin]; Data curation: [Ece Kutlu Narin]; Investigation: [Polat Narin], [Ece Kutlu Narin], [Sukru Ardali]; Writing-orginal draft: [Polat Narin], [Ece Kutlu Narin]; Poject admistration: [Sefer Bora Lisesivdin]; Writing-review & editing: [Beyza Sarikavak Lisesivdin], [Engin Tiras], [Sefer Bora Lisesivdin]

Funding Open access funding provided by the Scientific and Technological Research Council of Türkiye (TÜBİTAK).

Data availability Data will be made available at a reasonable request from the corresponding author.

Declarations

Conflict of interest The author(s) declared no potential conflicts of interest with respect to the research, authorship, and/or publication of this article.

Open Access This article is licensed under a Creative Commons Attribution 4.0 International License, which permits use, sharing, adaptation, distribution and reproduction in any medium or format, as long as you give appropriate credit to the original author(s) and the source, provide a link to the Creative Commons licence, and indicate if changes were made. The images or other third party material in this article are included in the article's Creative Commons licence, unless indicated otherwise in a credit line to the material. If material is not included in the article's Creative Commons licence and your intended use is not permitted by statutory regulation or exceeds the permitted use, you will need to obtain permission directly from the copyright holder. To view a copy of this licence, visit http://creativecommons.org/licenses/by/4.0/.

References

1. F. Bayat, S. Sheibani, Enhancement of photocatalytic activity of CuO-Cu2O heterostructures through the controlled content of Cu2O. Mater. Res. Bull. **145**, 111561 (2022)
2. T. Ha, I. Park, K.I. Sim, H. Lee, J.S. Bae, S.J. Kim, S.Y. Jeong, (2019). Single-crystalline Cu2O thin films of optical quality as obtained by the oxidation of single-crystal Cu thin films at low temperature. APL Mater. **7**(3)
3. M. Abdelfatah, W. Ismail, A. El-Shaer, Low cost inorganic white light emitting diode based on submicron ZnO rod arrays and electrodeposited Cu2O thin film. Mater. Sci. Semiconduct. Process. **81**, 44–47 (2018)
4. Q. Su, C. Zuo, M. Liu, X. Tai, A review on Cu2O-based composites in photocatalysis: synthesis, modification, and applications. Molecules. **28**(14), 5576 (2023)
5. J. Liu, S. Wang, Q. Wang, B. Geng, Microwave chemical route to self-assembled quasi-spherical Cu2O microarchitectures and their gas-sensing properties. Sens. Actuators B **143**(1), 253–260 (2009)
6. F. Marabelli, G.B. Parravicini, F.J.P.R.B. Salghetti-Drioli, Optical gap of CuO. Phys. Rev. B **52**(3), 1433 (1995)
7. J. Ghijsen, L.H. Tjeng, van J. Elp, H. Eskes, J. Westerink, G.A. Sawatzky, M.T. Czyzyk, Electronic structure of Cu 2 O and CuO. Phys. Rev. B **38**(16), 11322 (1988)
8. J. Kaur, A. Khanna, R. Kumar, R. Chandra, Growth and characterization of Cu2O and CuO thin films. J. Mater. Sci.: Mater. Electron. **33**(20), 16154–16166 (2022)
9. B. Maack, N. Nilius, Morphological and kinetic insights into Cu2O–CuO oxidation. Phys. status solidi (b). **257**(1), 1900365 (2020)
10. A. Eskandari, P. Sangpour, M.R. Vaezi, Hydrophilic Cu2O nanostructured thin films prepared by facile spin coating method: investigation of surface energy and roughness. Mater. Chem. Phys. **147**(3), 1204–1209 (2014)
11. T.H. Tran, V.T. Nguyen, Phase transition of Cu2O to CuO nanocrystals by selective laser heating. Mater. Sci. Semiconduct. Process. **46**, 6–9 (2016)
12. R.A. Abbas, E.T. Salim, R.O. Mahdi, Morphology transformation of Cu2O thin film: different environmental temperatures employing chemical method. J. Mater. Sci.: Mater. Electron. **35**(16), 1057 (2024)
13. D.S. Murali, S. Kumar, R.J. Choudhary, A.D. Wadikar, M.K. Jain, A. Subrahmanyam, (2015). Synthesis of Cu2O from CuO thin films: Optical and electrical properties. AIP Adv. **5**(4)
14. El W. Berjali, V. Colas, S.O.S. Hamady, S.S. Ng, N.A. Hamzah, P. Boulet, J.F. Pierson, (2025). Copper oxide by spin-coating: Cost-effective deposition and post-annealing process for thin films with modulated Cu2O/CuO phase ratio. Thin Solid Films. 140762
15. Y. Zhang, X. Xu, Machine learning band gaps of doped-TiO2 photocatalysts from structural and morphological parameters. ACS omega. **5**(25), 15344–15352 (2020)
16. Y. Zhang, X. Xu, Predicting the superconducting transition temperature and relative resistance ratio in YBa2Cu3O7 films. Physica C (Amsterdam, Neth.). **592**, 1353998 (2022)
17. S. Jeong, E.S. Aydil, Heteroepitaxial growth of Cu2O thin film on ZnO by metal organic chemical vapor deposition. J. Cryst. Growth. **311**(17), 4188–4192 (2009)
18. J.A. Kim, J.H. Park, S.G. Park, C.S. Son, Y.G. Son, D.H. Hwang, Effect of substrate temperature on variations in the structural and optical properties of Cu2O thin films deposited via RF magnetron sputtering. Crystals. **13**(4), 643 (2023)
19. P. Pattanasattayavong, S. Thomas, G. Adamopoulos, M.A. McLachlan, T.D. Anthopoulos, (2013). p-channel thin-film transistors based on spray-coated Cu2O films. Appl. Phys. Lett. **102**(16)
20. J. Jang, S. Chung, H. Kang, V. Subramanian, P-type CuO and Cu2O transistors derived from a sol–gel copper (II) acetate monohydrate precursor. Thin Solid Films. **600**, 157–161 (2016)
21. T. Sasaki, S. Kobayashi, T. Kouno, High-temperature growth of Cu2O crystals via mist chemical vapor deposition on Si (111) substrates. Jpn. J. Appl. Phys. **63**(12), 120903 (2024)
22. E. Kutlu-Narin, P. Narin, B. Emre, S.B. Lisesivdin, Influence of pH value of precursor on growth, structural, and optical properties of Cu2O thin films grown in Mist-CVD. Phys. B: Condens. Matter. **681**, 415860 (2024)
23. T. Ikenoue, T. Kawai, R. Wakashima, M. Miyake, T. Hirato, Hole mobility improvement in Cu2O thin films prepared by the mist CVD method. Appl. Phys. Express. **12**(5), 055509 (2019)

24. P. Wiecinski, A. Wieclaw-Midor, Metal salts as dopants for ZnO ceramics-thermogravimetry coupled with mass spectrometry studies. J. Therm. Anal. Calorim. **147**(10), 5599–5615 (2022)
25. D. Gupta, S.R. Meher, N. Illyaskutty, Z.C. Alex, Facile synthesis of Cu2O and CuO nanoparticles and study of their structural, optical and electronic properties. J. Alloys Compd. **743**, 737–745 (2018)
26. Y. Alajlani, F. Placido, H.O. Chu, De R. Bold, L. Fleming, D. Gibson, Characterisation of Cu2O/CuO thin films produced by plasma-assisted DC sputtering for solar cell application. Thin Solid Films. **642**, 45–50 (2017)
27. B. Maack, N. Nilius, Oxidation of polycrystalline copper films–Pressure and temperature dependence. Thin Solid Films. **651**, 24–30 (2018)
28. M.C. Kim, S.J. Kim, S.B. Han, D.H. Kwak, E.T. Hwang, D.M. Kim, K.W. Park, Cubic and octahedral Cu 2 O nanostructures as anodes for lithium-ion batteries. J. Mater. Chem. A **3**(45), 23003–23010 (2015)
29. J.R. Ares, A. Pascual, I.J. Ferrer, C. Sánchez, Grain and crystallite size in polycrystalline pyrite thin films. Thin Solid Films. **480**, 477–481 (2005)
30. K. Jrajri, M. Beraich, I. Warad, A. Guenbour, A. Bellaouchou, A. Zarrouk, Electrodeposition of Cu2O thin film onto copper substrate by linear sweep voltammetry at low duration: effect of bath pH. Biointerface Res. Appl. Chem. **12**(6), 7715–7724 (2022)
31. B.K. Meyer, A. Polity, D. Reppin, M. Becker, P. Hering, P.J. Klar, C. Ronning, Binary copper oxide semiconductors: From materials towards devices. Phys. status solidi (b). **249**(8), 1487–1509 (2012)
32. J.J.C.I. Chrzanowski, J.C. Irwin, Raman scattering from cupric oxide. Solid State Commun. **70**(1), 11–14 (1989)
33. A.E. Rakhshani, F.K. Barakat, Optical constants of reactively sputtered cupric oxide films. Mater. Lett. **6**(1–2), 37–40 (1987)
34. J.F. Pierson, A. Thobor-Keck, A. Billard, Cuprite, paramelaconite and tenorite films deposited by reactive magnetron sputtering. Appl. Surf. Sci. **210**(3–4), 359–367 (2003)
35. M. Balık, V. Bulut, I.Y. Erdogan, Optical, structural and phase transition properties of Cu2O, CuO and Cu2O/CuO: Their photoelectrochemical sensor applications. Int. J. Hydrog. Energy. **44**(34), 18744–18755 (2019)
36. A.L. Pellegrino, L. Presti, F. Smecca, E. Valastro, S. Greco, G. Di Franco, S. Malandrino, G, A low temperature growth of Cu2O thin films as hole transporting material for perovskite solar cells. Materials. **15**(21), 7790 (2022)
37. S. Bouachma, K. Ayouz-Chebout, M. Kechouane, A. Manseri, C. Yaddadene, H. Menari, N. Gabouze, Synthesis of PSi-n/CuO-p/Cu2O-n heterostructure for CO2 gas sensing at room temperature. Appl. Phys. A **128**(1), 69 (2022)
38. T. Ito, H. Yamaguchi, K. Okabe, T. Masumi, Single-crystal growth and characterization of Cu2O and CuO. J. Mater. Sci. **33**(14), 3555–3566 (1998)
39. H. Solache-Carranco, G. Juarez-Diaz, M. Galvan-Arellano, J. Martinez-Juarez, R. Pena-Sierra, (2008, November). Raman scattering and photoluminescence studies on Cu 2 O. In *2008 5th International Conference on Electrical Engineering, Computing Science and Automatic Control* (pp. 421–424). IEEE
40. R. Shabu, A.M.E. Raj, C. Sanjeeviraja, C. Ravidhas, Assessment of CuO thin films for its suitablity as window absorbing layer in solar cell fabrications. Mater. Res. Bull. **68**, 1–8 (2015)
41. P. Chand, A. Gaur, A. Kumar, Structural, optical and ferroelectric behavior of CuO nanostructures synthesized at different pH values. Superlattices Microstruct. **60**, 129–138 (2013)
42. M. Nolan, S.D. Elliott, The p-type conduction mechanism in Cu 2 O: a first principles study. Phys. Chem. Chem. Phys. **8**(45), 5350–5358 (2006)
43. J. Han, J. Chang, R. Wei, X. Ning, J. Li, Z. Li, Y. Yang, Mechanistic investigation on tuning the conductivity type of cuprous oxide (Cu2O) thin films via deposition potential. Int. J. Hydrogen Energy. **43**(30), 13764–13777 (2018)
44. M.A. Khalifa, M. Abdelfatah, M.A. Habib, A. El-Shaer, (2026). Revealing Defects in Cu2O microstructures: Temperature-Dependent Photoluminescence Insights from pH-Tuned Facet Engineering Cu2O. J. Lumin. 121751
45. Y. Zhang, X. Xu, Yttrium barium copper oxide superconducting transition temperature modeling through Gaussian process regression. Comput. Mater. Sci. **179**, 109583 (2020)
46. A. Sumanth, V. Mishra, P. Pandey, M.R. Rao, T. Dixit, Investigations into the role of native defects on photovoltaic and spintronic properties in copper oxide. IEEE Trans. Nanotechnol. **21**, 522–527 (2022)

Publisher's note Springer Nature remains neutral with regard to jurisdictional claims in published maps and institutional affiliations.